Journal of the Optical Society of America B
OPTICAL PHYSICS

Method of characterizing the multicomponent spectrum of a VCSEL in devices based on the CPT effect

D. Radnatarov, S. Kobtsev,* and V. Andryushkov

Division of Laser Physics and Innovative Technologies, Novosibirsk State University, Novosibirsk 630090, Russia
**Corresponding author: s.kobtsev@nsu.ru*

Received 2 September 2021; revised 5 October 2021; accepted 6 October 2021; posted 8 October 2021 (Doc. ID 442253); published 1 November 2021

We propose and experimentally demonstrate a method of spectral measurement of multicomponent radiation emitted by a modulated vertical cavity surface-emitting laser (VCSEL) relying on peculiarities of absorption in alkali metal vapor. The method consists in determination of the radiation spectrum (which is formed due to RF modulation of the injection current of a diode laser) from the dependence of transmittance of rubidium vapor upon the radiation wavelength. We show that the proposed method allows fairly precise measurement of the spectrum of multicomponent radiation used in devices based on the coherent population trapping (CPT) effect when the frequency difference between the radiation components matches that between absorption lines of an alkali metal.

https://doi.org/10.1364/JOSAB.442253

1. INTRODUCTION

Advancements in physics of interaction of resonant bichromatic radiation with alkali metal vapors and, in particular, the effect of coherent population trapping (CPT), as well as great progress in semiconductor lasers and high technologies, have resulted, over the last few decades, in development of miniaturized atomic frequency standards (AFS) [1–7]. Miniature AFS are widely used in embedded and wearable navigation and communication devices as well as in various research, engineering, and defense applications [8].

One of the key elements in such devices based on the CPT effect is a vertical-cavity surface-emitting diode laser (VCSEL) operating at a wavelength corresponding to that of the absorption line of an alkali metal (795 nm for ^{87}Rb). The modulation bandwidth of the diode laser must be broad enough (several GHz at a minimum) for simultaneous pumping of two atomic transitions resulting from hyperfine splitting [for example, $f_{\mathrm{HFS}} = 6.8$ GHz for ^{87}Rb, Fig. 1(a), or $f_{\mathrm{HFS}} = 9.2$ GHz for ^{133}Cs]. In order to produce in the laser radiation spectrum two frequencies differing by 6.8 or 9.2 GHz, its injection current is modulated at the frequency equal to half that of hyperfine splitting of the ground level of the alkali atom [3.4 or 4.6 GHz, Fig. 1(b)]. The two-photon CPT resonance is formed by the -1 and $+1$ spectral components tuned to transitions b and d. Modulation can also be performed at lower fractional frequencies ($f_{\mathrm{HFS}}/3$, $f_{\mathrm{HFS}}/4$, etc.); most often, however, half-frequency is used (3.4 or 4.6 GHz).

As the VCSEL's injection current is modulated at a frequency f, additional components emerge in the output spectrum spaced from their neighbors by f. Initially, a single-frequency spectrum of the laser becomes multifrequency, and its measurement normally requires either high-finesse Fabry–Perot interferometers [9,10] or optical heterodyning [11]. We would like to show, however, that another way of laser spectrum measurement exists (applicable also for finding the distribution of intensity among spectral components) that does not require any external equipment.

The properties of CPT resonances and, in particular, their amplitude, light field shift, and the shape symmetricity depend on the intensity distribution of the radiation spectral components [12–14]. These properties may equally depend on other factors (magnitude and direction of magnetic field, polarization state of radiation, buffer gas pressure in the optical cell [15], and so on); therefore, it is important that the laser output spectrum be readily and easily measurable. The present work was motivated by the question of whether it was possible to determine the laser output spectrum by its absorption in alkali metal vapor. This work positively demonstrates such a possibility, and the limitations thereof are analyzed later on in the Discussion.

The idea consists in recording the radiation absorption spectrum by tuning the laser's wavelength so that the resulting spectrum is affected by the maximum spectral components of the laser radiation. This resulting spectrum is a convolution of each spectral component of the laser radiation with the absorption spectrum [Fig. 1(c)]; further, if the absorption spectrum

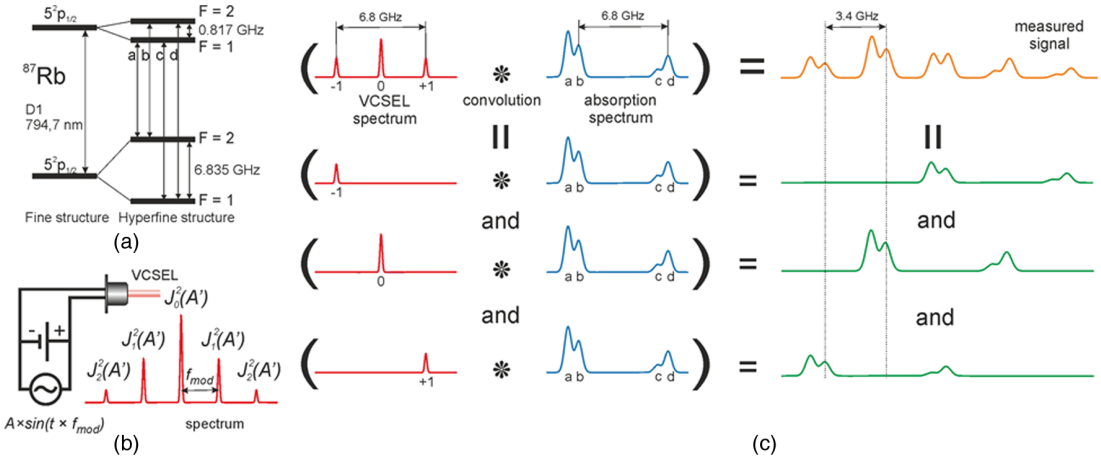

Fig. 1. (a) Level structure of the D1 line in ^{87}Rb. (b) Transformation of single-frequency radiation into a multicomponent one by modulation of the pumping laser's injection current. J_n^2 is the squared Bessel function of the first kind, n referring to the order of the spectral component, A′ is the amplitude of phase modulation, linearly dependent on A, which is the amplitude of laser current modulations at small A. (c) Formation of the absorption signal with multicomponent radiation (for illustrative purposes, only three components are shown; in a general case, their number is not limited); the measured signal is a convolution of the laser output spectrum and that of the atomic absorption. It may be represented as a sum of convolutions resulting from each spectral component of radiation whose frequency continuously changes when scanning the atomic absorption spectrum.

is already known, it may be subjected to the inverse procedure of deconvolution. The absorption spectrum may be obtained directly by scanning the output wavelength of the laser with no current modulation (corresponding to single-frequency operation). It should be taken into consideration, however, that both the amplitude and shape of the absorption spectrum depend on the radiation intensity [16].

For the first time, to the best of our knowledge, this work demonstrates the possibility of qualitative measurement of the spectrum of multifrequency output of a VCSEL by its absorption in an alkali metal vapor.

2. EXPERIMENTAL SETUP

For measurement of the VCSEL's output spectrum, an experimental installation was put together (Fig. 2) on the basis of a laboratory atomic frequency standard (AFS) using the CPT effect earlier described in [17,18]. This configuration was significantly different from the standard optical layout conventionally used in AFS in that linear radiation polarization was used instead of circular. This was done in order to eliminate the effect of optical pumping upon the shape of absorption lines [19], in which circularly polarized radiation travelling along the magnetic field direction causes redistribution of ground-state electrons among Zeeman sublevels, resulting in nonlinear reduction of absorption. Our experiments were conducted on

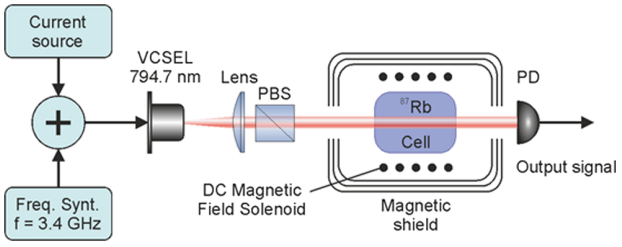

Fig. 2. Experimental setup: PBS, polarizer; PD, photodetector.

a 7 mm long optical cell with an antirelaxation coating of its internal walls [20]. Compared with a buffer gas cell, in such cells there is almost no impact broadening of the absorption line Doppler contour [21,22], to those that allow resolving the hyperfine structure of the excited state [Fig. 1(a)] and detailed characterization of the spectrum. Cell temperature has been stabilized at ∼ 50°C. The intensity of the magnetic field was 50 mG.

The radiation wavelength was scanned by adjustment of the VCSEL injection current. A typical dependence of the photodetector signal registering the intensity of the radiation transmitted through the optical cell is presented in Fig. 3(a). This specific measurement was performed at the laser radiation power of 5 μW. As one can see from the graph, the dependence $PD(I)$ has a constant slope whose presence arises from the fact that not only the radiation wavelength $\lambda(I)$ but also its power Power(I) depend on the injection current, both dependencies being linear to a high degree of precision. This allows easy removal of the slope in this dependency during data processing. Since the output power changes significantly when adjusting the wavelength, the radiation power is understood as the power emitted at a certain injection current (for instance, at the current of 2.75 mA, at which the transmission spectrum has the deepest dip).

The atomic absorption signal was calculated as Absorption$(I) = -(PD(I) - \text{Power}(I))$ [removal of Power(I) slope in Fig. 3(a)]. Conversion to the frequency domain of the dependence Absorption$(I) \rightarrow$ Absorption(Δf) was done, taking into account the fact that the frequency difference between transitions a and c equals 6.835 GHz, the origin being placed at the frequency of transition a. The dependence of the absorption signal upon the frequency detuning at the radiation power of 5 μW is presented in Fig. 3(b) (blue curve).

As it can be seen from this figure, apart from the peaks corresponding to transitions $a - d$ in ^{87}Rb, the spectrum contains additional relatively small peaks. These peaks form a structure

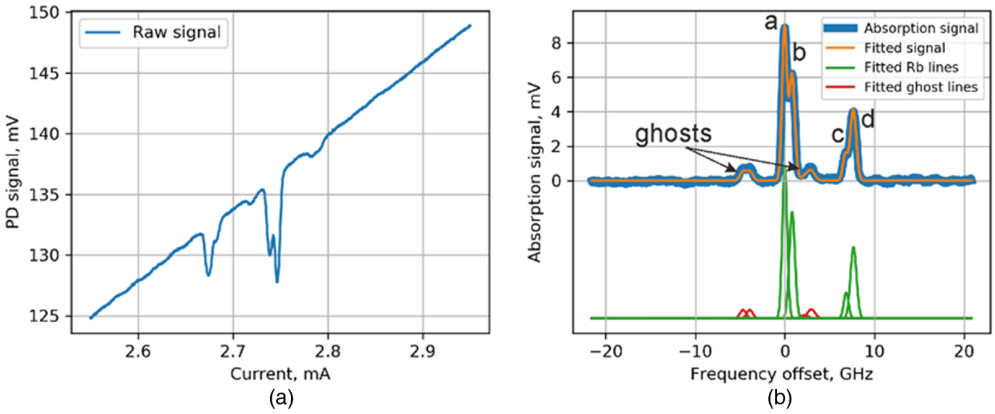

Fig. 3. Absorption spectrum of the D1 line in ^{87}Rb at the radiation power of 5 μW. (a) Photodetector signal as a function of the VCSEL current. (b) Absorption spectrum (blue curve is the measured absorption spectrum; orange curve is the spectrum approximation; green curve is the approximation of individual absorption contours of ^{87}Rb; red curve is the approximation of the secondary peaks [for illustrative purposes, individual transition contours are shifted]).

similar to that of peaks corresponding to transitions $a - d$ (double peaks spaced by 6.8 GHz with the subpeaks at 0.8 GHz from each other), but shifted toward lower frequencies by ∼ 4.5 GHz. Positions of these peaks indicate that they cannot correspond to the lines of the stable rubidium isotope ^{85}Rb. Our conjecture is that this series of peaks corresponds to absorption lines of a special ^{87}Rb ensemble whose atoms are embedded into the thickness of paraffin antirelaxation coating of the cell walls [23] and experience additional influence from the coating that shifts the transition frequency. The number of atoms thus embedded is relatively small, which is corroborated by the fact that the contour of these secondary lines did not depend upon the radiation power within the measured range, indicating that these absorption lines were saturated.

3. CHARACTERIZATION OF THE RADIATION SPECTRUM

Implementation of the proposed method of spectral characterization of multicomponent radiation is done in two steps. (1) Calibration, i.e., measurement of the dependence of the absorption peak parameters upon the intensity of single-frequency radiation, from which a function is constructed that depends upon the radiation intensity and serves to approximate the absorption spectrum at an arbitrary intensity of the single-frequency radiation. This step is necessary because both height and width of the peaks forming the absorption spectrum depend upon the radiation intensity [16], and each component of multifrequency radiation will generate an absorption spectrum depending on its intensity. (2) Approximation, i.e., approximation of the multicomponent radiation spectrum that consists in finding out the number and intensities of the radiation spectral components. The objective is to arrive at the sum of spectral profiles generated by each radiation component that is as close as possible to the measured dependence.

4. CALIBRATION

To measure the dependence of the absorption peak parameters upon the radiation intensity, the absorption spectrum of the optical cell with ^{87}Rb was registered at several levels of the optical radiation power in the range of 2 to 7 μW. Each of these spectra contains eight peaks, of which four peaks with the highest magnitude correspond to transitions $a - d$ of the primary atomic ensemble, while four secondary peaks arise from the atoms embedded into the wall coating. For measurement of parameters of these peaks, each spectrum was approximated by a function representing a sum of eight Gaussian contours (each for one observed peak): four contours for the peaks $a - d$ [green curves in Fig. 3(b)] and four other contours for the secondary peaks [red curves in Fig. 3(b)]. Each contour had a specific shift that was determined by the known transition frequency difference [Fig. 1(b)] and the measured shift of the secondary peak structure (−4.5 GHz):

$$\text{Absorption}_{\text{fit}}(\Delta f) = \sum_{i}^{4} G\,(A_i, \omega_i, f_i, \Delta f) + \sum_{k}^{4} G\,(A_k, \omega_k, f_k, \Delta f)\,,$$

where $G(A, \omega, \Delta f, \Delta f) = A \cdot \exp\left(-(\Delta f - f)/\omega\right)^2)$ is the Gaussian contour with parameters: A is the peak height, f is the peak position, and ω is the peak half width; $i = a, b, c, d$ is the index corresponding to the primary absorption peaks; $k = a', b', c', d'$ is the index of the secondary absorption peaks. As the approximation parameters of each peak were chosen for height and half width, the peak positions were set manually. It should be noted that, in the general case, the Voigt contour [16] should rather be used for the approximation. However, in the specific case of an antirelaxation-coated optical cell, it was revealed that the simplified Gaussian approximation is sufficient. This may happen because the natural absorption line width in alkali metals is much narrower than that of the Doppler contour [16]; hence, the shape of the Voigt contour, which is a convolution of a Lorentz contour with the natural width and a Doppler Gaussian contour, is only determined by the Doppler broadening and can be described by a Gaussian profile to a high precision. Additionally, antireflection-coated cells do not contain any buffer gas that could produce impact broadening of the line. Time-of-flight broadening is also small

(<1 MHz) and does not appreciably affect the absorption line contour. The resulting approximation function is shown as the orange curve in Fig. 3(b). Data processing was performed with software written in Python language. Approximation was done with the function "curve_fit" from the standard "scipy" library.

Because the parameters of the absorption line contour depend upon the radiation power, the corresponding dependencies were measured of the parameters A_i, ω_i, A_k, and ω_k. The registered dependencies were then fitted as follows: a linear function was used for the contour width parameter $\omega_i(P)$ [Fig. 4(a)], a third-power polynomial with a fixed root at *(0, 0)* was chosen for amplitude $A_i(P)$ [Fig. 4(b)]. In the fitting process, we took into consideration the dependence of the radiation power upon the frequency detuning Power(Δf) that arises because the radiation power also depends upon the laser injection current [Fig. 3(a)], i.e., at $i > 0$, it was necessary to use $P_i' = \text{Power}(f_i)$. Because neither amplitude nor shape of the secondary peaks depended upon the radiation power, our approximation took their width as constant, whereas their amplitude was linearly dependent upon the power in the range of 0 to 1 μW and constant at powers exceeding 1 μW.

As a result, the following approximation function was calculated where the dependence of the peak absorption shape upon the radiation intensity was factored in

$$\text{Absorption}_{\text{fit}}(\Delta f,\ f_{\text{shift}},\ P) = \sum_i^4 G\big(A_i(P),\ \omega_i(P),\ f_i + f_{\text{shift}},\ \Delta f\big) + \sum_k^4 G\big(A_k(P),\ \omega_k(P),\ f_k + f_{\text{shift}},\ \Delta f\big).$$

This function also contains a frequency shift f_{shift}, which will be needed later for approximation of signals resulting from multicomponent radiation. Because the frequency of the spectral side peaks is shifted with respect to the central one, the absorption peaks resulting from them are also shifted [see Fig. 1(c)].

5. APPROXIMATION OF MULTICOMPONENT ABSORPTION SPECTRUM

Further on, we measured and fitted multicomponent absorption spectra generated with modulation of the laser current by an RF signal of varying power (Fig. 5).

For approximation of the generated spectra, the following expression was used, which is the sum of functions produced at the previous step:

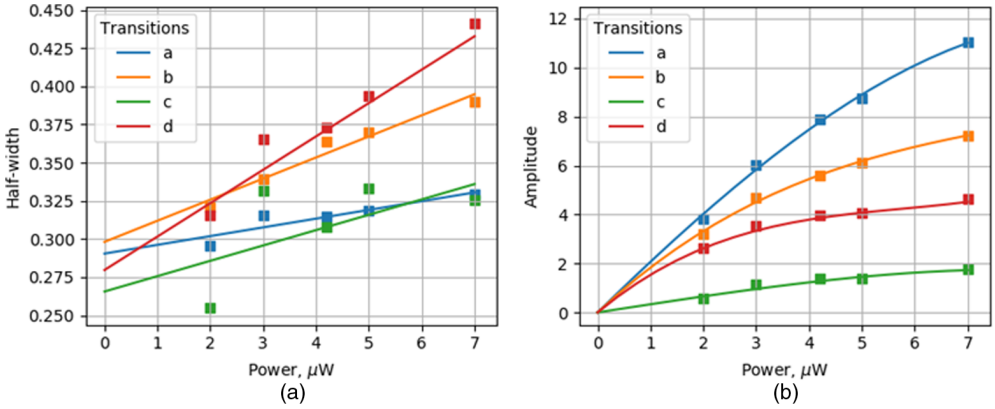

Fig. 4. Dependence upon the optical radiation power of the fitting parameters of the absorption line contours. For fitting of the dependence of the contour width upon power, a linear function was used, whereas a third-power polynomial with a root at the origin was taken for the contour amplitude.

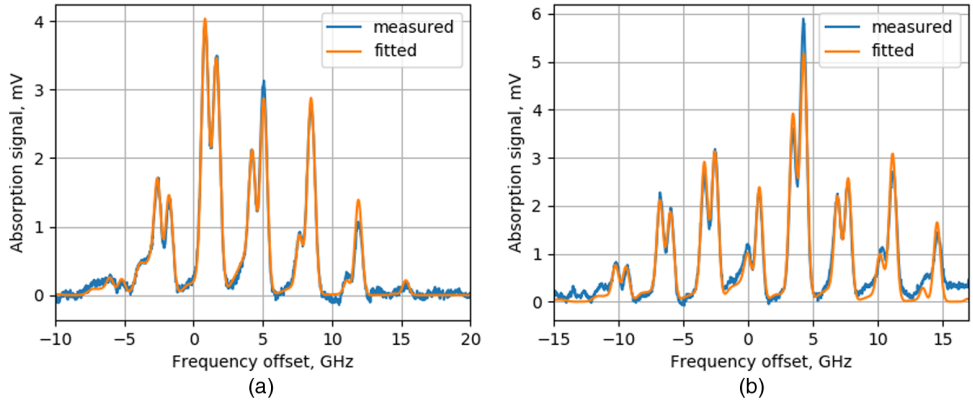

Fig. 5. Absorption spectra (dependence of the absorption signal upon the detuning of the central wavelength of the laser radiation) at powers of modulation signal (a) −10 dBm and (b) −2 dBm. Blue curves are for experimental dependencies; orange curves are for the final approximation.

$$\text{Multiabsorption}_{\text{fit}}(\Delta f) = \sum_{s} \text{Absorption}_{\text{fit}}\left(\Delta f,\ f_{\text{shift}}(s),\ p_s\right),$$

where $s = -s_{\max}, \ldots, 0, \ldots, s_{\max}$ is the spectral component index, $s_{\max}$ is the highest order of the spectral component that may be estimated as $N_{\text{peaks}}/2 + 1$, where N_{peaks} is the number of double peak structures observed within the multicomponent spectrum, $f_{\text{shift}}(s) = f_{\text{HFS}}/2 \times s$ is the frequency shift of the dependence, which is determined by the shift of the spectral frequency component s with respect to the central one, p_s is the intensity of the radiation spectral component that we are looking for. Here, as well as in the process of absorption line approximation, we also factored in the dependence of the radiation power upon frequency, in this case upon $f_{\text{shift}}(s)$. This step was also carried out with the help of function "curve_fit" from the standard "scipy" library. The time required for fitting of a single multicomponent absorption spectrum did not exceed 15–20 s when performed on a desktop computer with an Intel Core i5 processor.

Figure 5 demonstrates the intensity distribution of spectral components calculated as presented above in the case of the VCSEL injection current modulated with a low-power signal (−10 dBm) and close to the normal operation power (−2 dBm). The operation power is understood as the modulation signal power, at which the light field shift of the CPT resonance is compensated and, consequently, the best long-term stability achieved for an atomic clock based on this effect.

The obtained results illustrated in Fig. 6 meet our expectations. It can be seen that, at a small modulation amplitude, the spectrum is symmetrical, which is typical in the case of low-power phase modulation when the amplitude of the spectral side peaks drops quickly as their order grows. At modulation amplitude close to normal for operation, the number of spectral components grows, and the amplitude of the central component is considerably lower than that of the neighboring ±1 components that are the highest. Such amplitude distribution is also expected, taking into account that the calculated value of the modulation amplitude at which the light shift is eliminated [24] is close to that, at which the central component is suppressed and the neighboring ±1 components reach their highest level [4]. Spectral asymmetry, which is most clearly visible in the neighboring ±1 components, is an equally expected effect; at higher modulation amplitude, there also emerges amplitude modulation that leads to different amplitudes of the symmetrical components [11]. Thus, a preliminary conclusion may be drawn that the laser spectrum measured by the proposed method is rather realistic.

6. METHOD VALIDATION

For comparison of the radiation spectrum calculated as proposed with a similar spectrum measured differently (for instance, by optical heterodyning), the following experiment was conducted whose diagram is presented in Fig. 7. In this experiment, the laser output spectrum was detected with the help of a different single-frequency laser whose frequency was scanned, while the beat signal of these two laser outputs was recorded within a narrow frequency band (down to 1 MHz). In order to deliver the radiation of the studied laser to the experiment location, we used a multimode optical fiber with a 150 μm core. Because this fiber did not maintain polarization, the polarization of both lasers' radiation was converted to circular with phase plates. Further on, the beams from both lasers were superimposed on each other through a beam-splitting plate (50:50) and directed onto a photodetector with a 5 MHz bandwidth. The AC component of the photodetector signal was boosted with a preamplifier and digitized with a 14-bit ADC at the rate of 10 MS/s, the photodetector signal being collected for 50 ms. After that, the signal was filtered within the frequency pass band of 50 kHz–1 MHz for removal of lower frequencies and reduction of extraneous noises. In such a beat signal registration method, the detector output signal has linear dependence upon the intensities of both laser beams. This fact was verified by taking the detector signal amplitude at different intensities of the scanning laser.

The comparison results are presented in Fig. 8. One can see that the calculated values are quite close to the real ones and reflect correctly the qualitative picture: at low amplitude of modulation, the height of the symmetrical spectral components is equal, while at high modulation amplitude, an asymmetry is introduced into the spectrum that results from amplitude modulation [9,11]. It may be noted that the developed method of spectral measurement reports the difference in the intensities of the ±1 spectral components quite precisely, which is important because it is these specific components that participate in excitation of the reference resonance in devices based on the

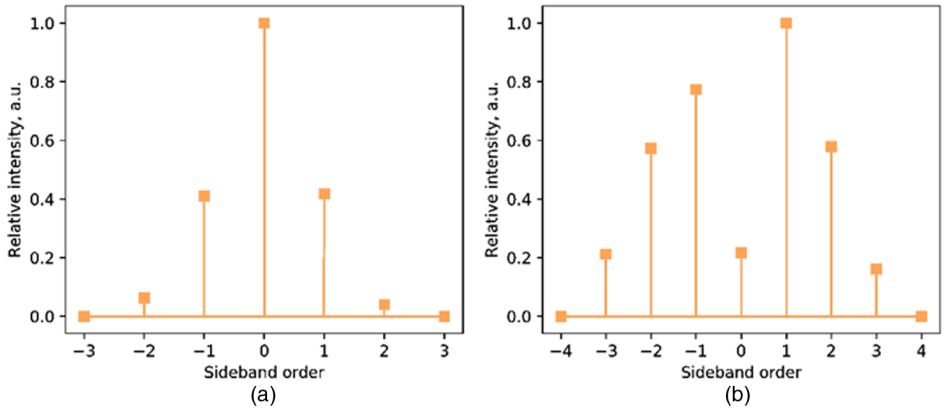

Fig. 6. Calculated VCSEL spectrum at the modulation signal power (a) −10 dBm and (b) −2 dBm.

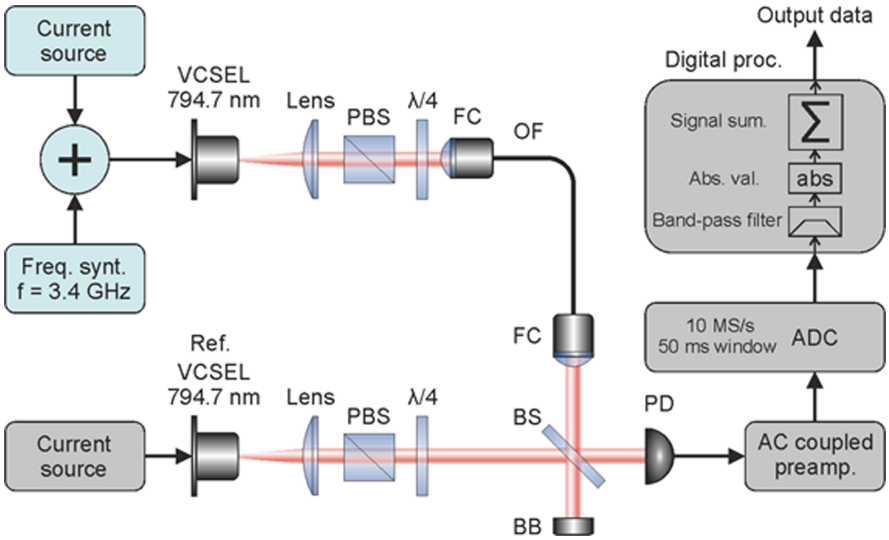

Fig. 7. Setup by laser heterodyning. PBS, polarizer; FC, fiber collimator; λ/4, quarter-wave plate; OF, multimode optical fiber; BS, beam splitter (50:50); BB, beam block; PD, photodetector.

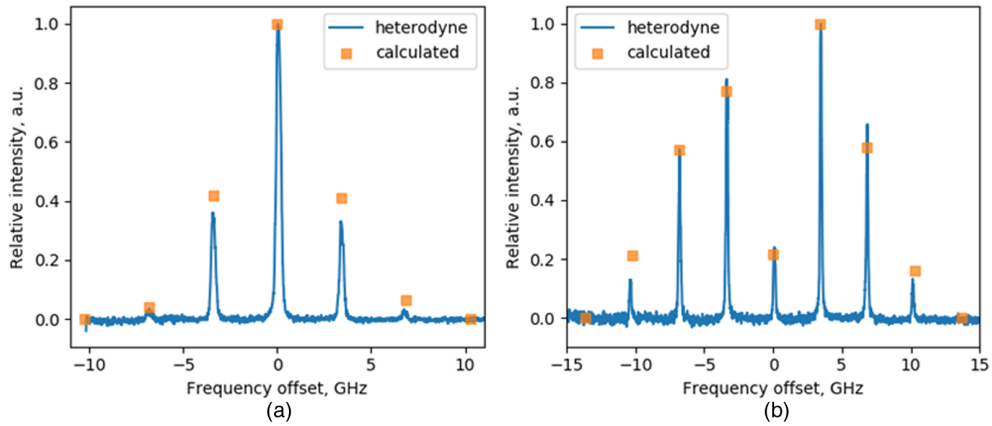

Fig. 8. Comparison of the results of VCSEL's spectrum characterisation calculated from approximations of multicomponent spectrum with results of spectrum measurement by method of optical heterodyning.

CPT effect, while a large difference in their intensity results in the resonance asymmetry, which may detrimentally affect the stability of atomic frequency standards [14].

7. DISCUSSION

The results obtained in this work indicate that the spectrum of multicomponent laser radiation may be reconstructed from the absorption contour shape, provided that the dependencies of the parameters of absorption line contours upon the radiation intensity are known and the lines are resolved. The key point here is the demonstrated possibility of decomposition of the measured absorption contour into a linear combination of absorption spectra resulting from radiation components with different intensity. This raises hopes that the proposed method may be also applied in devices using optical cells with buffer gas where impact broadening may lead to the Doppler contour width exceeding that of the hyperfine splitting frequency of the excited state. In this case, the impossibility of resolving all the transitions may, likely, affect the precision of the extracted spectral component amplitudes, but the qualitative analysis of the spectrum will be still possible in regard to the number of the components, relative amplitudes of symmetrical components, and the presence/absence in the spectrum of ghost lines [11]. It is also possible to use circular polarization of radiation that is necessary in real-life devices based on the CPT effect. During measurement, the effect of optical pumping on the absorption spectrum may be eliminated by turning off the magnetic field, for instance.

Among the factors that are able to affect the accuracy of the presented method, one should note optical absorbance of the medium. We are of the opinion that this method is applicable at any temperatures useable in CPT devices (40°C–90°C) but is most accurate within approximately the range of 40°C–60°C for optical cells of subcentimeter dimensions, which correspond to low optical absorption when the radiation intensity changes weakly across the cell, but the contrast of the peaks is sufficient for their identification and measurement against the photodetector noise. In our measurements, the cell temperature was 50°C, and the cell absorption did not exceed 4%; that is, the

absorption could be neglected. At higher cell temperatures, when absorbance become significant, it is necessary to take into consideration the fact that the absorption peaks will be deformed because the radiation intensity changes along the beam path, and, as demonstrated earlier, the width and height of the absorption contour depend upon the radiation intensity. Nonetheless, on the one hand, all the deformations of the absorption contours arising from the medium absorbance may be factored in during calibration, when measuring the dependence of the width and height of the absorption contours upon the radiation intensity. On the other hand, it may be conjectured that, at higher atomic densities, the accuracy of the method could be compromised because of higher nonlinearities in the dependencies of absorption profile parameters. That is why, in order to extract the most accurate information about the VCSEL spectrum, both calibration and measurement should be carried out at such optical cell temperature as to ensure that the medium absorbance may be neglected. This may likely be realized in real-life devices based on the CPT effect.

It should be further pointed out that the origin of the secondary absorption peaks present in our experiments is not entirely understood. On the one hand, the structure and shift sign of these peaks indicate their relation to rubidium atoms embedded into the thickness of the paraffin coating of the inside walls of the optical cell. However, the spectral width of these peaks is comparable with that of the absorption peaks in atomic vapor within the cell's volume, i.e., it is too small for absorption peaks that may be observed in solid state. We are not aware of any publications proposing a model that would allow calculation of absorption line profiles of atoms trapped in the paraffin coating. Hence, a separate study of this question is necessary, which falls outside the scope of the present work. It may be noted, though, that, according to the available data [21,22], the impact shift of absorption lines in rubidium interacting with organic compounds is negative, which agrees with our results.

The other possible origin of the secondary peaks may be the initial presence of more than one frequency in the VCSEL output. Such nonsingle-frequency generation may have led to the observed structure of absorption peaks at fixed radiation intensity, but this would not explain why the amplitude of the secondary peaks did not depend on the radiation intensity. Neither did direct measurement of the laser output spectrum via optical heterodyning suggest presence of additional lines in the laser's generation spectrum.

Finding out the cause of these peaks requires additional separate research, because it would be highly desirable to create devices with the active atoms embedded into the paraffine thickness and not subject to interactions leading to absorption line broadening, such as solid-state frequency standards and magnetometers. As far as the present work is concerned, however, it may be noted that the origin of the secondary peaks is of no major importance for implementation of the proposed method.

8. CONCLUSION

A new method is proposed for characterization of the spectrum of multicomponent laser radiation generated under RF modulation of a diode laser (VCSEL) injection current in devices based on the CPT effect in alkali metal vapors. This method does not require any additional spectral equipment (e.g., interferometers), relies on measured dependence of the absorption line contours upon the radiation intensity, and allows precise characterization of the radiation spectrum.

Further development of this method includes its adaptation to devices using optical cells with buffer gas and circular polarization of radiation. This work presents a proof of concept demonstrating the possibilities of the proposed method for "built-in" characterization of a multicomponent radiation spectrum.

Funding. Russian Science Foundation (21-12-00057); Ministry of Science and Higher Education of the Russian Federation (FSUS-2020-0036); Russian Foundation for Basic Research (18-29-20025).

Disclosures. The authors declare no conflicts of interest.

Data Availability. Data underlying the results presented in this paper are not publicity available at this time but may be obtained from the authors upon reasonable request.

REFERENCES

1. J. Kitching, "Chip-scale atomic devices," Appl. Phys. Rev. **5**, 031302 (2018).
2. J. Vanier, "Atomic clocks based on coherent population trapping: a review," Appl. Phys. B **81**, 421–442 (2005).
3. R. Lutwak, P. Vlitas, M. Varghes, M. Mescher, D. K. Serkland, and G. M. Peake, "The MAC—a miniature atomic clock," in *Proceedings of the 2005 IEEE International Frequency Control Symposium and Exposition* (IEEE, 2005), pp. 752–757.
4. N. Cyr, M. Tetu, and M. Breton, "All-optical microwave frequency standard: a proposal," IEEE Trans. Instrum. Meas. **42**, 640–649 (1993).
5. W. Zhong, "Review of chip-scale atomic clocks based on coherent population trapping," Chin. Phys. B **23**, 030601 (2014).
6. S. A. Zibrov, V. L. Velichansky, A. S. Zibrov, A. V. Taichenachev, and V. I. Yudin, "Experimental investigation of the dark pseudoresonance on the D_1 line of the ^{87}Rb atom excited by a linearly polarized field," J. Exp. Theor. Phys. Lett. **82**, 534–538 (2005).
7. S. A. Zibrov, I. Novikova, D. F. Phillips, R. L. Walsworth, A. S. Zibrov, V. L. Velichansky, A. V. Taichenachev, and V. I. Yudin, "Coherent-population-trapping resonances with linearly polarized light for all-optical miniature atomic clocks," Phys. Rev. A **81**, 013833 (2010).
8. J. R. Vig, "Military applications of high accuracy frequency standards and clocks," IEEE Trans. Ultrason. Ferroelectr. Freq. Control **40**, 522–527 (1993).
9. M. I. Vas'kovskaya, V. V. Vasil'ev, S. A. Zibrov, V. P. Yakovlev, and V. L. Velichanskii, "Spectral-modulation characteristics of vertical-cavity surface-emitting lasers," Tech. Phys. Lett. **44**, 20–23 (2018).
10. C. M. Long and K. D. Choquette, "Optical characterization of a vertical cavity surface emitting laser for a coherent population trapping frequency reference," J. Appl. Phys. **103**, 033101 (2008).
11. A. O. Makarov, S. M. Ignatovich, V. I. Vishnyakov, I. S. Mesenzova, D. V. Brazhnikov, N. L. Kvashnin, and M. N. Skvortsov, "Investigation of commercial 894.6 nm vertical-cavity surface-emitting lasers for applications in quantum metrology," AIP Conf. Proc. **2098**, 020010 (2019).
12. S. M. Ignatovich, V. I. Vishnyakov, A. O. Makarov, M. N. Skvortsov, N. L. Kvashnin, V. A. Vasiliev, S. N. Atutov, D. V. Brazhnikov, V. I. Yudin, A. V. Taichenachev, and S. N. Bagayev, "CPT atomic clock based on an antirelaxation-coated cell and quadrature-signal method of the light shift cancellation," in *European Frequency and Time Forum (EFTF)* (IEEE, 2018), pp. 83–86.
13. D. S. Chuchelov, V. V. Vassiliev, M. I. Vaskovskaya, V. L. Velichansky, E. A. Tsygankov, S. A. Zibrov, S. V. Petropavlovsky, and V. P. Yakovlev, "Modulation spectroscopy of coherent population trapping resonance and light shifts," Phys. Scr. **93**, 114002 (2018).
14. D. S. Chuchelov, E. A. Tsygankov, M. I. Vaskovskaya, S. A. Zibrov, V. L. Velichansky, S. V. Petropavlovsky, and V. P. Yakovlev, "Study of

factors affecting the light shift of the CPT resonance," J. Phys. Conf. Ser. **1686**, 012029 (2020).
15. M. I. Vaskovskaya, E. A. Tsygankov, D. S. Chuchelov, S. A. Zibrov, V. V. Vassiliev, and V. L. Velichansky, "Effect of the buffer gases on the light shift suppression possibility," Opt. Express **27**, 35856–35864 (2019).
16. W. Demtröder, *Laser Spectroscopy: Basic Concepts and Instrumentation*, 3rd ed. (Springer, 2013).
17. S. Khripunov, D. Radnatarov, and S. Kobtsev, "Atomic clock based on a coherent population trapping resonance in ^{87}Rb with improved high-frequency modulation parameters," Proc. SPIE **9378**, 93780A (2015).
18. D. Radnatarov, S. M. Kobtsev, V. Andryushkov, and S. Khripunov, "Features of a CPT-based atomic clock with pumping by different-order sidebands of a VCSEL's frequency," Proc. SPIE **11195**, 111950Y (2019).
19. W. Happer, "Optical pumping," Rev. Mod. Phys. **44**, 169–250 (1972).
20. M. V. Balabas, K. Jensen, W. Wasilewski, H. Krauter, L. S. Madsen, J. H. Müller, T. Fernholz, and E. S. Polzik, "High quality anti-relaxation coating material for alkali atom vapor cells," Opt. Express **18**, 5825–5830 (2010).
21. M. D. Rotondaro and G. P. Perram, "Collisional broadening and shift of the rubidium D_1 and D_2 lines by rare gases, H_2, D_2, N_2, CH_4 and CF_4," J. Quant. Spectrosc. Radiat. Transfer **57**, 497–507 (1997).
22. G. A. Pitz, A. J. Sandoval, T. B. Tafoya, W. L. Klennert, and D. A. Hostutler, "Pressure broadening and shift of the rubidium D_1 transition and potassium D_2 transitions by various gases with comparison to other alkali rates," J. Quant. Spectrosc. Radiat. Transfer **140**, 18–29 (2014).
23. S. N. Atutov, F. A. Benimetskiy, A. I. Plekhanov, V. A. Sorokin, and A. V. Yakovlev, "Diffusion of Rb atoms in paraffin-coated resonant vapor cells," Eur. Phys. J. D **71**, 12 (2017).
24. M. Zhu and L. S. Cutler, "Theoretical and experimental study of light shift in a CPT-based Rb vapor cell frequency standard," in *Proc. of the 32nd Annual Precise Time and Time Interval (PTTI) Meeting* (2000), pp. 311–323.